

The building blocks of planets within the 'terrestrial' region of protoplanetary disks

R. van Boekel^{1,2}, M. Min¹, Ch. Leinert³, L.B.F.M. Waters^{1,4}, A. Richichi², O. Chesneau³, C. Dominik¹, W. Jaffe⁵, A. Dutrey⁶, U. Graser³, Th. Henning³, J. de Jong⁵, R. Köhler³, A. de Koter¹, B. Lopez⁷, F. Malbet⁵, S. Morel², F. Paresce², G. Perrin⁸, Th. Preibisch⁹, F. Przygodda³, M. Schöller² & M. Wittkowski²

- ¹Astronomical Institute "Anton Pannekoek", University of Amsterdam, Kruislaan 403, 1098 SJ Amsterdam, The Netherlands
- ²European Southern Observatory, Karl-Schwarzschild-Strasse 2, D-85748 Garching, Germany
- ³Max-Planck-Institut für Astronomie Heidelberg, Königstuhl 17, 69117 Heidelberg, Germany
- ⁴Instituut voor Sterrenkunde, K.U. Leuven, Celestijnenlaan 200B, 3001 Heverlee, Belgium
- ⁵Leiden Observatory, Niels Bohrweg 2, 2333 CA Leiden, The Netherlands
- ⁶Observatoire de Bordeaux 2, rue de l'Observatoire F-33270 Floirac, France
- ⁷Observatoire de la Côte d'Azur, Département Fresnel UMR 6528, BP 4229, 06034 Nice Cedex 4, France
- ⁸Laboratoire d'Etudes Spatiales et d'Instrumentation en Astrophysique, Observatoire de Paris, section de Meudon, 5 place Jule Janssen, 92190 Meudon, France
- ⁹Max-Planck-Institut für Radioastronomie, Auf dem Hügel 69, 53121 Bonn, Germany

Our Solar System was formed from a cloud of gas and dust. Most of the dust mass is contained in amorphous silicates¹, yet crystalline silicates are abundant throughout the Solar System, reflecting the thermal and chemical alteration of solids during planet formation. (Even primitive bodies such as comets contain crystalline silicates².) Little is known about the evolution of the dust that forms Earth-like planets. Here we report spatially resolved detections and compositional analyses of these building blocks in the innermost two astronomical units of three protoplanetary disks. We find the dust in these regions to be highly crystallized, more so than any other dust observed in young stars until now. In addition, the outer region of one star has equal amounts of pyroxene and olivine, whereas the inner regions are dominated by olivine. The spectral shape of the inner-disk spectra shows surprising similarity with Solar System comets. Radial-mixing models naturally explain this resemblance as well as the gradient in chemical composition. Our observations imply that silicates crystallize before any terrestrial planets are formed, consistent with the composition of meteorites in the Solar System.

Most young stars are surrounded by a disk of gas and dust which is a remnant of the star-formation process. This disk is formed owing to conservation of angular momentum in the collapsing proto-stellar cloud, and channels material from the cloud to the proto-star. When the material in the surrounding molecular cloud is exhausted, the disk dissipates within approximately 10⁷ years (ref. 3). Planet formation is believed to result from the growth of submicrometre-sized interstellar dust particles⁴. Therefore, changes in size but also in the chemical nature of the dust grains in the nebular disk environment trace the first steps in planet formation. For instance, crystalline silicates are formed as a result of thermal annealing of amorphous grains, or by vaporization and subsequent gas-phase condensation in the innermost disk regions. These are referred to as primary processes. After inclusion of dust in larger parent bodies such as asteroids and planets, so-called secondary processing occurs, which includes oxidation, aqueous alteration and thermal metamorphism. Asteroids and comets contain pristine

interstellar dust as well as dust which has seen substantial processing⁵. The reconstruction of the formation history of our Solar System depends on a better understanding of the nature of primary and secondary processes, and when and where they occurred in the proto-solar nebula.

We observed three Herbig Ae stars with the Mid-Infrared Interferometric Instrument (MIDI)⁶ installed at the Very Large Telescope Interferometer (VLTI). The light from two 8.2-m Unit Telescopes separated by 103 m on the ground was combined, providing a spatial resolution of about 20 milli-arcseconds. This corresponds to ~1–2 astronomical units (AU) at the distance of the observed stars; an improvement of more than a factor of ten in spatial resolution compared to the largest modern-day telescopes, in this wavelength regime. The MIDI instrument measures spectrally dispersed visibilities with $\lambda/\Delta\lambda = 30$ in the 7.5–13.5- μm atmospheric window. The intensity distribution of circumstellar disks is strongly centrally peaked^{7,8}, so the correlated spectra measured by the interferometer are dominated by the inner 1–2 AU of the disks. We refer to these as the inner-disk spectra. In addition, spectra were obtained with a single 8.2-m telescope, in which the objects are spatially unresolved⁸. We refer to these spectra as the total-disk spectra. The difference between the total- and the inner-disk spectra arises mainly from a region between approximately 2 and 20 AU. We will refer to these spectra as the outer-disk spectra.

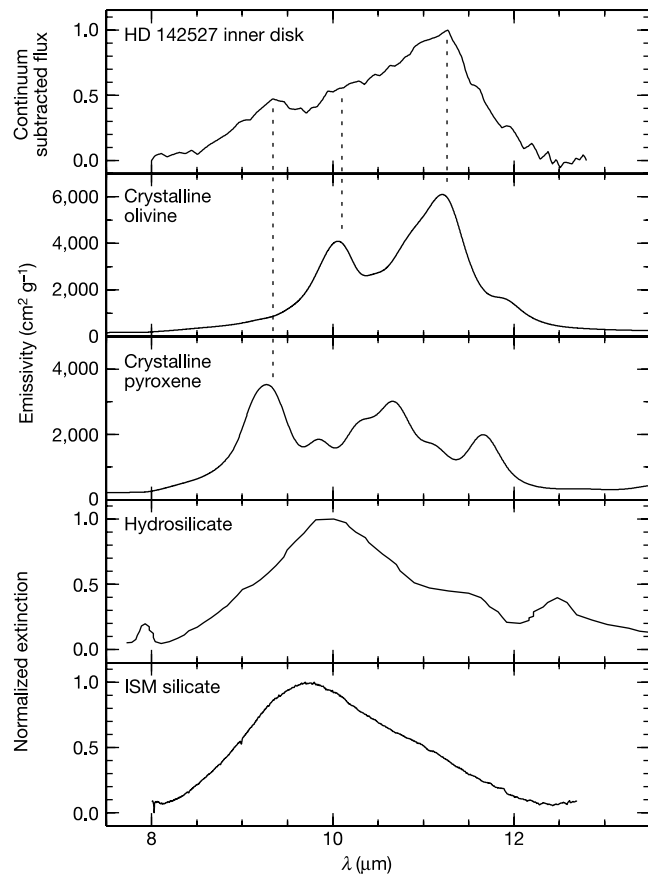


Figure 1 The spectrum of the innermost disk regions of HD 142527 compared to spectra of typical dust species. From top to bottom we plot the observed inner-disk spectrum of HD 142527, the laboratory spectra of crystalline olivine and pyroxene²⁹, a laboratory spectrum of an IDP consisting of hydrated silicates¹⁷, and the interstellar medium silicate spectrum¹. The resolution of the laboratory data is reduced to that of the interferometric spectrum. The main resonances of crystalline pyroxene at 9.2 μm and crystalline olivine at 11.3 μm are clearly seen in the HD 142527 spectrum. We can exclude the possibility of a significant contribution of hydrated silicates to the spectrum in the inner-disk regions of HD 142527, which suggests that we see primary, rather than secondary dust.

In Fig. 1 we show the inner-disk spectrum of HD 142527. The spectrum is clearly dominated by crystalline olivine and pyroxene. These minerals are also the most common in Solar System objects. No contribution from amorphous silicates is evident. As shown below, the spectrum is in fact consistent with 100 per cent crystalline material, making it the most crystalline dust ever observed in young stars⁹. Clearly, the mechanism responsible for crystallization must be highly efficient. Figure 2 shows the inner- and outer-disk spectra for all three stars. We have fitted the observations using laboratory measurements of materials that are the dominant species found in circumstellar disks¹⁰ and interplanetary dust particles⁵. The derived mass fraction of crystalline silicates, the olivine over pyroxene ratio in the inner- and outer-disk spectra, and the fraction of material that resides in large grains, are listed in Table 1.

Both in the Solar System and in circumstellar disks crystalline silicates are found at large distances from the star. The origin of these silicates is a matter of debate. Although in the hot inner-disk

regions crystalline silicates can be produced by means of gas-phase condensation or thermal annealing, the typical grain temperatures in the outer-disk (2–20 AU) regions are far below the glass temperature of silicates of ~1,000 K. The crystals in these regions may have been transported outward through the disk¹¹ or in an outward-flowing wind¹². An alternative source of crystalline silicates in the outer disk regions is *in situ* annealing, for example by shocks¹³ or lightning^{14,15}. A third way to produce crystalline silicates is the collisional destruction of large parent bodies in which secondary processing has taken place. We can use the mineralogy of the dust to derive information about the nature of the primary and/or secondary processes the small-grain population has undergone.

Models of disks accounting for the chemical equilibrium of a solid-gas mixture at high temperatures as well as the radial mixing of material¹¹ predict that the innermost disk region consists entirely of forsterite (the Mg-rich end member of the olivine family). At slightly lower temperatures, a reaction with gas-phase silicon efficiently converts this to enstatite (the Mg-rich end member of the pyroxene family). At a larger distance from the star, the predicted crystalline olivine over pyroxene ratio reaches about 0.5. Our observations qualitatively confirm these predictions. The inner-disk spectrum of HD 142527 imposes the strongest constraints because it shows the most-processed dust in our data. Assuming equal temperatures for all dust species, we find that the ratio of olivine to pyroxene in the inner-disk spectrum is 2.1, whereas it is 0.9 in the outer-disk spectrum. To our knowledge, this is the first direct measurement of a gradient in the chemical composition of the dust in proto-planetary disks. The measured gradient is smaller than is predicted by radial-mixing models. This could be due to non-equilibrium chemistry, or to the assumed stoichiometry in the amorphous silicates prior to annealing.

For all three stars the inner-disk regions have a substantially higher degree of crystallinity than the outer regions. However, these outer regions show a crystalline silicate abundance that clearly exceeds limits derived for the interstellar medium¹. Therefore, these crystalline silicates must have been produced in the disk. It is not clear that the local processes that have been proposed to produce these crystals can account for the observed degree of crystallinity. Models for radial mixing of proto-planetary disks¹¹ can produce a crystalline fraction of several tens of per cent at distances of 5–10 AU (which is the relevant scale for our

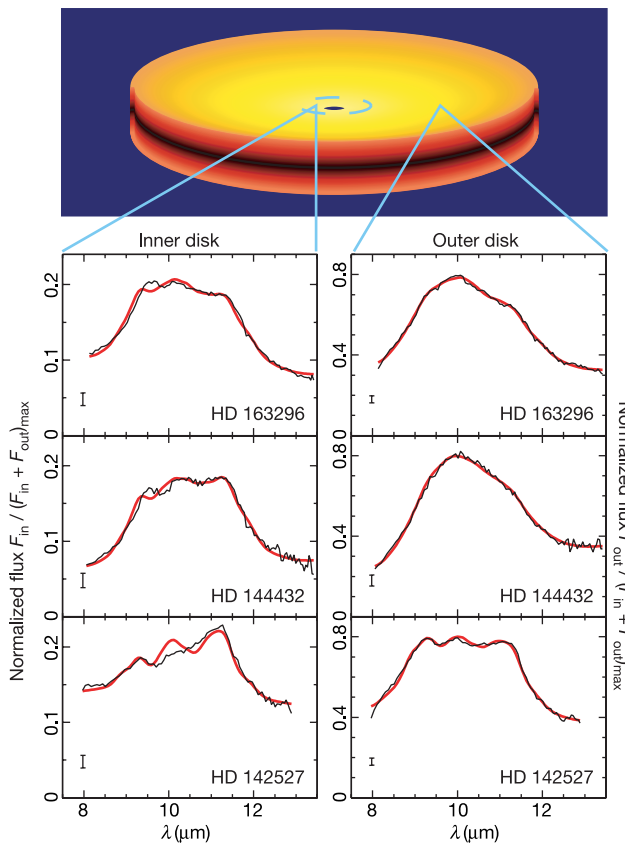


Figure 2 Infrared spectra of the inner (1–2 AU) and outer (2–20 AU) disk regions of three Herbig Ae stars. The outer-disk spectrum of each source has been constructed by subtracting the correlated spectrum from the total-disk spectrum (see ref. 8). The regions that dominate the inner- and outer-disk spectra are indicated in the schematic representation of a proto-planetary disk at the top of the figure (not to scale). The flux levels are scaled such that the sum of the inner- and outer-disk spectrum, that is, the total-disk spectrum, is normalized to unity. This allows the relative contributions of the inner and outer disk to the total spectrum to be estimated easily from this figure. The uncertainties in the spectra are indicated by the error bars in the lower left corner of each graph. The differences in shape between the inner- and outer-disk spectra are clearly visible in all three sources, indicating a difference in dust mineralogy. The broadening of the feature as seen in the inner-disk spectra indicates grain growth, whereas the resonance at 11.3 μm indicates the presence of crystalline silicates (see also Fig. 1). Also shown are the best-fit model spectra for the inner- and outer-disk regions (red lines, see also Table 1). The model spectra reproduce the observed spectral shapes, although the fits to the inner disk spectra are less good than the fits to the outer-disk spectra.

Table 1 Dust properties in the inner and outer disk

	Crystallinity (%)		Fraction of large grains (%)		Crystalline olivine to pyroxene ratio	
	Inner disk	Outer disk	Inner disk	Outer disk	Inner disk	Outer disk
HD 163296	40 ⁺²⁰ ₋₂₀	15 ⁺¹⁰ ₋₁₀	95 ⁺⁵ ₋₁₀	65 ⁺²⁰ ₋₂₀	2.3 ^{+3.7} _{-0.5}	–
HD 144432	55 ⁺³⁰ ₋₂₀	10 ⁺¹⁰ ₋₅	90 ⁺¹⁰ ₋₁₀	35 ⁺²⁰ ₋₂₀	2.0 ^{+1.8} _{-0.6}	–
HD 142527	95 ⁺⁵ ₋₁₅	40 ⁺²⁰ ₋₁₅	65 ⁺¹⁵ ₋₁₀	80 ⁺¹⁰ ₋₃₀	2.1 ^{+1.3} _{-0.7}	0.9 ^{+0.2} _{-0.1}

The fractional abundances of large and crystalline grains as well as the ratio of crystalline olivine to pyroxene in the inner (1–2 AU) and outer (2–20 AU) disk regions of three Herbig Ae stars. The dust components used in the model spectra are amorphous and crystalline olivine ($\text{Mg}_2\text{Fe}_{2-2}\text{SiO}_4$), amorphous and crystalline pyroxene ($\text{Mg}_x\text{Fe}_{1-x}\text{SiO}_3$), and amorphous silica (SiO_2). For the crystalline components we used the magnesium-rich silicates ($x = 1$) and for the amorphous components we used $x = 0.5$. The crystallinity is defined as the percentage of the total dust mass contributing to the 10- μm feature, contained in crystalline olivine and pyroxene. Because the signature of crystalline silicates in the outer disk spectra of HD 163296 and HD 144432 is not very clear, the ratio of crystalline olivine over pyroxene in these spectra is not very well determined. The abundance of crystalline pyroxene in these spectra is particularly poorly constrained. All dust species are considered to have two different grain sizes, 0.1 μm (small grains) and 1.5 μm (large grains). Because we are looking at a coagulating environment where the various dust species are expected to be in thermal contact, we assume that all components have the same temperature. The opacities of the dust species are calculated from refractive indices obtained by laboratory measurements^{24–27}, using the method of ref. 28. The abundances of the various dust species are determined using a linear least-squares fitting procedure assuming the dust emission comes from an optically thin part of the disk. The errors on the fitting parameters include both uncertainties in the data and in the modelling method, and are 1σ . As most of the error budget is due to systematic uncertainties that are the same in the inner and outer disk spectra, the relative difference between the two is much more significant than the error bars suggest. For details on the fitting procedure and the error analysis see the Supplementary Information.

observations), provided that a reservoir of crystalline material is present in the innermost disk regions. Our data prove that this reservoir exists.

Secondary processing of dust in large parent bodies produces hydrous silicates by means of aqueous alteration. Studies of meteorites have shown that the fine-grained matrix material of chondrites often consists of hydrous silicates¹⁶. However, we can exclude the possibility that the grains in our sources are predominantly hydrosilicates, because these show a fairly sharp peak near 10 μm , as seen in interplanetary dust particles (IDPs) rich in hydrosilicates¹⁷. We conclude that aqueous alteration, followed by parent-body destruction, has not yet resulted in the production of a large abundance of small hydrosilicate grains in HD 142527. Therefore, parent-body processing can be excluded as the main source of crystalline silicates.

Figure 3 shows a remarkable similarity between the inner-disk spectra of our objects and those of Solar System comets, suggesting that the composition of the dust is also comparable. Therefore, the building blocks of comets in our Solar System have been processed in a similar way and to the same degree as in the inner disks of our programme stars. This is surprising, because comets formed in the icy regions of the solar nebula, further than 5 AU from the Sun. Cometary crystalline silicates are Mg-rich¹⁸. Chemical-equilibrium models indeed predict the formation of Mg-rich crystalline silicates at very high temperatures¹¹. Measurements of the composition of

crystalline silicates that form in the outflows of red giants¹⁹ support such chemical models. In addition, crystalline silicates found in fluffy, chondritic IDPs have a whisker or platelet morphology and internal crystallographic defects, indicative of gas-phase condensation⁵. This latter process is unlikely to occur in the outer regions of proto-planetary disks, but is expected to be important in the innermost regions. The most natural explanation for the presence of these materials in comets therefore seems to be transport by radial mixing from the rich reservoir of processed, Mg-rich crystalline silicate grains in the inner disk. Furthermore, radial-mixing models can account for the presence of cold crystalline silicates in the outer (> 20 AU) regions of some proto-planetary disks^{10,20} as well as the occurrence of large (10–20 μm) FeS crystals in IDPs of cometary origin⁵.

It has been suggested that the degree of crystallinity of proto-planetary disks slowly increases with time after the accretion of matter on the star has stopped²¹. This evidence is based on the lack of crystalline silicates in infrared spectra of embedded young stars in the active phase, which are still accreting gas and dust from an interstellar cloud²². In contrast, passive proto-planetary disks around optically visible stars that are no longer accreting matter can show strong crystalline silicate emission²⁰. The star with the highest abundance of crystalline silicates in our sample, HD 142527, is also the youngest one, with an age of approximately 1 million years (R.v.B. *et al.*, manuscript in preparation). Our observations thus imply that crystallization of almost the entire inner disk and a substantial part of the outer disk must have occurred very early in the evolution of the disk. Because dust processing—both radial mixing and shock processing—is more efficient during the active-disk phase, our observations provide strong evidence that crystallization occurred in the active-disk phase. The formation of the planets and asteroids in the inner Solar System is believed to have occurred on a much longer timescale²³, during the passive disk phase. Therefore, our observations indicate that, as was the case in the early Solar System¹⁶, the silicate dust in the inner regions of proto-planetary disks is highly crystalline before planet formation occurs. □

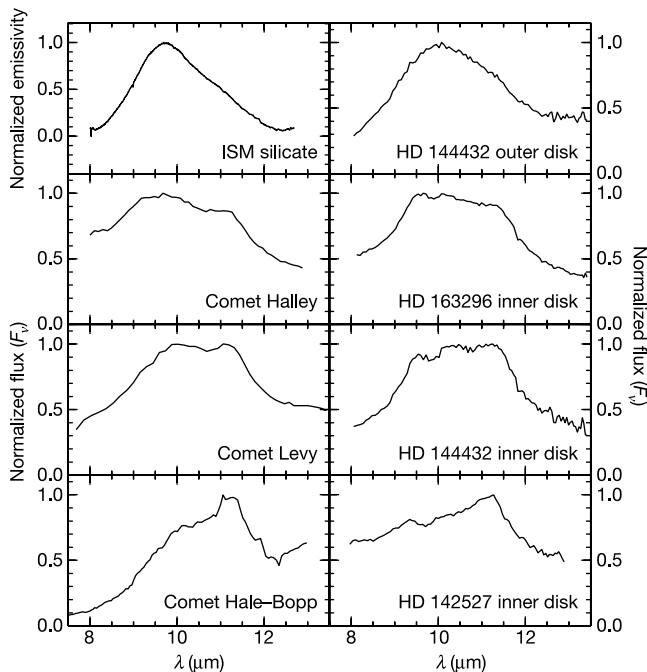


Figure 3 A comparison between the spectral shapes of various astronomical objects (left column) with those of the inner- and outer-disk regions of our three Herbig Ae stars (right column). In the first row, we compare the silicate feature of the interstellar medium (ISM¹) with the outer-disk spectrum of HD 144432. The silicate grains in the ISM are small (<0.1 μm) and amorphous. This results in a spectrum that has a typical triangular shape, peaking at 9.7 μm . The outer-disk spectrum of HD 144432 is very similar, although a very weak shoulder at 11.3 μm can be seen, indicating the presence of small amounts of processed material. In the second to the last rows, we compare the inner-disk spectra of our three Herbig stars with three Solar System comets^{2–18}. The shapes of these spectra are very different from that of the ISM, indicating a higher degree of crystallinity, and on average larger dust grains. Grain growth makes the silicate emission band broader. Crystalline silicates have several bands in the 8–13- μm spectral region, the strongest of which is at 11.3 μm . Modest crystallinity causes the silicate feature to have rather sharp shoulders around 9.5 and 11.5 μm , whereas in highly crystalline sources the crystalline silicates show prominent peaks (see Hale Bopp and HD 142527). The spectra are shown here in order of increasing crystallinity from top to bottom.

Received 5 May; accepted 5 October 2004; doi:10.1038/nature03088.

- Kemper, F., Friend, W. J. & Tielens, A. G. G. M. The absence of crystalline silicates in the diffuse interstellar medium. *Astrophys. J.* **609**, 826–837 (2004).
- Hanner, M. S., Lynch, D. K. & Russell, R. W. The 8–13 micron spectra of comets and the composition of silicate grains. *Astrophys. J.* **425**, 274–285 (1994).
- Haisch, K. E., Lada, E. A. & Lada, C. J. Disk frequencies and lifetimes in young clusters. *Astrophys. J. Lett.* **533**, L153–L156 (2001).
- Beckwith, S. V. W., Henning, T. & Nakagawa, Y. Dust properties and assembly of large particles in protoplanetary disks. In *Protostars and Planets IV* (eds Mannings, V., Boss, A. P. & Russell, S. S.) 533–558 (Univ. Arizona Press, 2000).
- Bradley, J. in *Lecture Notes in Physics* Vol. 609 *Astromineralogy* (ed. Henning, Th.) 217–235 (2003).
- Leinert, C. *et al.* Ten-micron instrument MIDI: getting ready for observations on the VLTI. in *Interferometry for Optical Astronomy II* (ed. Traub, W.A.). *Proc. SPIE* **4838**, 893–904 (2003).
- Eisner, J. A., Lane, B. F., Akeson, R. L., Hillenbrand, L. A. & Sargent, A. I. Near-infrared interferometric measurements of Herbig Ae/Be Stars. *Astrophys. J.* **588**, 360–372 (2003).
- Leinert, C. *et al.* Mid-infrared sizes of circumstellar disks around Herbig Ae/Be stars measured with MIDI on the VLTI. *Astron. Astrophys.* **423**, 537–548 (2004).
- Molster, F. J. & Waters, L. B. F. M. in *Lecture Notes in Physics* Vol. 609 *Astromineralogy* (ed. Henning, Th.) 121–170 (2003).
- Bouwman, J. *et al.* Processing of silicate dust grains in Herbig Ae/Be systems. *Astron. Astrophys.* **375**, 950–962 (2001).
- Gail, H.-P. Radial mixing in protoplanetary accretion disks. IV. Metamorphosis of the silicate dust complex. *Astron. Astrophys.* **413**, 571–591 (2004).
- Nuth, J. A., Rietmeijer, F. J. M. & Hill, H. G. M. Condensation processes in astrophysical environments: The composition and structure of cometary grains. *Meteorit. Planet. Sci.* **37**, 1579–1590 (2002).
- Harker, D. E. & Desch, S. J. Annealing of silicate dust by nebular shocks at 10 AU. *Astrophys. J. Lett.* **565**, L109–L112 (2002).
- Pilipp, W., Hartquist, T. W., Morfill, G. E. & Levy, E. H. Chondrule formation by lightning in the Protosolar Nebula? *Astron. Astrophys.* **331**, 121–146 (1998).
- Desch, S. J. & Cuzzi, J. N. The generation of lightning in the solar nebula. *Icarus* **143**, 87–105 (2000).
- Brearely, A. & Jones, R. H. in *Planetary Materials* (ed. Papike, J.) Ch. 3 (The Mineralogical Society of America, 1998).
- Sandford, S. A. & Walker, R. M. Laboratory infrared transmission spectra of individual interplanetary dust particles from 2.5 to 25 microns. *Astrophys. J.* **291**, 838–851 (1985).

18. Crovisier, J. *et al.* The spectrum of Comet Hale-Bopp (C/1995 01) observed with the Infrared Space Observatory at 2.9 AU from the Sun. *Science* **275**, 1904–1907 (1997).
19. Molster, F. J., Waters, L. B. F. M., Tielens, A. G. G. M., Koike, C. & Chihara, H. Crystalline silicate dust around evolved stars. III. A correlations study of crystalline silicate features. *Astron. Astrophys.* **382**, 241–255 (2002).
20. Malfait, K. *et al.* The spectrum of the young star HD 100546 observed with the Infrared Space Observatory. *Astron. Astrophys.* **332**, L25–L28 (1998).
21. Grady, C. A. *et al.* Infalling planetesimals in pre-main stellar systems. In *Protostars and Planets IV* (eds Mannings, V., Boss, A. P. & Russell, S. S.) 613–638 (Univ. Arizona Press, 2000).
22. Acke, B. & van den Ancker, M. E. ISO spectroscopy of disks around Herbig Ae/Be stars. *Astron. Astrophys.* (in the press); preprint at (<http://xxx.lanl.gov/astro-ph/0406050>) (2004).
23. Wetherill, G. W. Formation of the earth. *Annu. Rev. Earth Planet. Sci.* **18**, 205–256 (1990).
24. Dorschner, J., Begemann, B., Henning, T., Jäger, C. & Mutschke, H. Steps toward interstellar silicate mineralogy. *Astron. Astrophys.* **300**, 503–520 (1995).
25. Servoin, J. L. & Piriou, B. Infrared reflectivity and Raman scattering of Mg₂SiO₄ single crystal. *Phys. Status Solidi* **55**, 677–686 (1973).
26. Jäger, C. *et al.* Steps toward interstellar silicate mineralogy. IV. The crystalline revolution. *Astron. Astrophys.* **339**, 904–916 (1998).
27. Spitzer, W. G. & Kleinman, D. A. Infrared lattice bands of quartz. *Phys. Rev.* **121**, 1324–1335 (1961).
28. Min, M., Hovenier, J. W. & de Koter, A. Shape effects in scattering and absorption by randomly oriented particles small compared to the wavelength. *Astron. Astrophys.* **404**, 35–46 (2003).
29. Chihara, H., Koike, C. & Tsuchiyama, A. Low-temperature optical properties of silicate particles in the far-infrared region. *Publ. Astron. Soc. Jpn* **53**, 243–250 (2001).

Supplementary Information accompanies the paper on www.nature.com/nature.

Acknowledgements The data is based on observations obtained at the European Southern Observatory (ESO), Chile. We thank all those involved in building VLTI and MIDI. We thank V. Icke for providing the illustration shown in Fig. 2. C.P. Dullemond is acknowledged for many discussions.

Competing interests statement The authors declare that they have no competing financial interests.

Correspondence and requests for materials should be addressed to R.v.B. (vboukel@science.uva.nl).

Experimental demonstration of quantum memory for light

Brian Julsgaard¹, Jacob Sherson^{1,2}, J. Ignacio Cirac³, Jaromir Fiurášek⁴ & Eugene S. Polzik¹

¹Niels Bohr Institute, Danish Quantum Optics Center – QUANTOP, Copenhagen University, Blegdamsvej 17, 2100 Copenhagen Ø, Denmark

²Department of Physics, Danish Quantum Optics Center – QUANTOP, University of Aarhus, 8000 Aarhus C, Denmark

³Max Planck Institute for Quantum Optics, Hans-Kopfermann-Str. 1, Garching, D-85748, Germany

⁴QUIC, Ecole Polytechnique, CP 165, Université Libre de Bruxelles, 1050 Brussels, Belgium, and Department of Optics, Palacky University, 17. listopadu 50, 77200 Olomouc, Czech Republic

The information carrier of today's communications, a weak pulse of light, is an intrinsically quantum object. As a consequence, complete information about the pulse cannot be perfectly recorded in a classical memory, even in principle. In the field of quantum information, this has led to the long-standing challenge of how to achieve a high-fidelity transfer of an independently prepared quantum state of light onto an atomic quantum state^{1–4}. Here we propose and experimentally demonstrate a protocol for such a quantum memory based on atomic ensembles. Recording of an externally provided quantum state of light onto the atomic quantum memory is achieved with 70 per cent fidelity, significantly higher than the limit for classical recording. Quantum storage of light is achieved in three steps: first, interaction of the input pulse and an entangling field with spin-polarized caesium atoms; second, subsequent measurement of the transmitted light; and third, feedback onto the atoms using a radio-frequency magnetic pulse conditioned on the measure-

ment result. The density of recorded states is 33 per cent higher than the best classical recording of light onto atoms, with a quantum memory lifetime of up to 4 milliseconds.

Light is a natural carrier of information in both classical and quantum communications. In classical communications, bits are encoded in large average amplitudes of light pulses, which are detected, converted into electric signals and subsequently stored as charges or magnetization of memory cells. In quantum information processing, information is encoded in quantum states that cannot be accurately recorded by such classical means. Consider a state of light defined by its amplitude and phase, or equivalently by two quadrature phase operators, \hat{X}_L and \hat{P}_L , with the canonical commutation relation $[\hat{X}_L, \hat{P}_L] = i$. These variables play the same role in quantum mechanics as the classical quadratures X, P do in the decomposition of the electric field of light with the frequency ω as $E \propto X \cos \omega t + P \sin \omega t$. Other quantum properties of light, such as the photon number $\hat{n} = \frac{1}{2}(\hat{X}_L^2 + \hat{P}_L^2 - 1)$, and so on, can be expressed in terms of \hat{X}_L and \hat{P}_L .

The best classical approach to recording a state of light onto atoms would involve homodyne measurements of both observables \hat{X}_L and \hat{P}_L by using, for example, a beam splitter. The non-commutativity of \hat{X}_L and \hat{P}_L leads to additional quantum noise being added during this procedure. The target atomic state has its intrinsic quantum noise (coming from the Heisenberg uncertainty relations). All this extra noise leads to a limited fidelity for the classical recording: for example, to a maximum fidelity of 50% for coherent states^{5–7}. Thus the challenge of implementing a quantum memory can be formulated as a faithful storing of the simultaneously immeasurable values of \hat{X}_L and \hat{P}_L .

A number of quantum information protocols, such as eavesdropping in quantum cryptography, quantum repeaters⁸, and linear optics quantum computing⁹, would benefit from a memory meeting the following criteria: (1) the light pulse to be stored is sent by a third party in a state unknown to the memory party; (2) the state of light is converted into a quantum state of the memory with a fidelity higher than that of the classical recording. Several recent experiments^{10–13} have demonstrated entanglement of light and atoms. However, none of these experiments demonstrated memory obeying the two above criteria. In ref. 14, where squeezed light was mapped onto atoms, the atomic state existed only while the light was on, so it was not a memory device. The electromagnetically induced transparency (EIT) approach has led to the demonstration of a classical memory for light^{15,16}. A theoretical proposal for EIT-based quantum memory for light has been published in ref. 3. Other proposals for quantum memory for light with better-than-classical quality of recording have also been published recently^{1–4}.

Quantum state transfer from one species to another is most simply presented if both systems are described by canonical quantum variables \hat{X}, \hat{P} . All canonical variables have the same commutation relations and the same quantum noise for a given state, thus providing a common frame for the analysis of the state transfer.

In the present work, the state of light is stored in the superposition of magnetic sublevels of the ground state of an atomic ensemble. As in ref. 12, we introduce the operator \hat{J} of the collective magnetic moment (orientation) of a ground state F . All atomic states utilized here are not too far in phase space from the coherent spin state (CSS), for which only one projection has a non-zero mean value, for example, $\langle \hat{J}_x \rangle = J_x$, whereas the other two projections have minimal quantum uncertainties, $\langle \delta \hat{J}_y^2 \rangle = \langle \delta \hat{J}_z^2 \rangle = \frac{1}{2} J_x$. For all such states, the commutator $[\hat{J}_y, \hat{J}_z] = i \hat{J}_x$ can be reduced to the canonical commutator $[\hat{X}_A, \hat{P}_A] = i$ with $\hat{X}_A = \hat{J}_y / \sqrt{J_x}$, $\hat{P}_A = \hat{J}_z / \sqrt{J_x}$. Hence the y, z -components of the collective atomic angular momentum play the role of canonical variables. Although the memory protocol, in principle, can work with a single atomic ensemble, experimental technical noise is substantially reduced if two oppositely polarized ensembles placed in a bias magnetic field \mathbf{H} are used (see Methods